Title
Asymptotic high-frequency Green's function for a planar phased sectoral array of dipoles

Journal
Radio Science, 35(2)

ISSN
0048-6604

Authors
Capolino, F
Maci, S
Felsen, LB

Publication Date
2000-03-01

DOI
10.1029/1999rs900107

Radio Science, Volume 35, Number 2, Pages 579–593, March–April 2000

Asymptotic high-frequency Green's function for a planar phased sectoral array of dipoles

F. Capolino and S. Maci

Department of Information Engineering, University of Siena, Siena, Italy

L. B. Felsen

Departments of Aerospace and Mechanical Engineering and Electrical and Computer Engineering
Boston University, Boston, Massachusetts

Abstract. This paper deals with the derivation and physical interpretation of a uniform high-frequency Green's function for a planar right-angle sectoral phased array of dipoles. This high-frequency Green's function represents the basic constituent for the full-wave description of electromagnetic radiation from rectangular periodic arrays and scattering from rectangular periodic structures. The field obtained by direct summation over the contributions from the individual radiators is restructured into a double spectral integral whose high-frequency asymptotic reduction yields a series of propagating and evanescent Floquet waves (FWs) together with corresponding FW-modulated diffracted fields, which arise from FW scattering at the array edges and vertex. Emphasis is given to the analysis and physical interpretation of the vertex diffracted rays. The locally uniform asymptotics governing this phenomenology is physically appealing, numerically accurate, and efficient, owing to the rapid convergence of both the FW series and the series of corresponding FW-modulated diffracted fields away from the array plane. A sample calculation is included to demonstrate the accuracy of the asymptotic algorithm.

1. Introduction

In the electromagnetic modeling of large phased arrays, which is a topic of current interest [*Ishimaru et al.*, 1985; *Skrivervik and Mosig*, 1992; *Felsen and Carin*, 1994; *Carin and Felsen*, 1993; *Felsen and Gago Ribas*, 1996; *Capolino et al.*, 1998; *Neto et al.*, 1998; *Civi et al.*, 1998], one objective [*Ishimaru et al.*, 1985; *Skrivervik and Mosig*, 1992; *Neto et al.*, 1998] is to reduce the often prohibitive numerical effort that accompanies an element-by-element full-wave analysis based on integral equations which are structured around the ordinary free-space Green's function; when applied to a periodic array, this array Green's function is composed of the sum over the individual dipole radiations. As an alternative, we explore replacement of the element-by-element Green's function by the array Green's function (AGF), which represents the collective field radiated by the elementary dipoles. The efficient calculation of the AGF is accomplished via a Floquet wave (FW) representation like that proposed by *Felsen and Carin* [1994], *Carin and Felsen* [1993], *Felsen and Gago Ribas* [1996], and *Capolino et al.* [1998]. With this representation, the radiation from, or scattering by, finite phased arrays is interpreted as the radiation from a superposition of continuous equivalent FW-matched source distributions extending over the entire finite array aperture. The asymptotic treatment of each FW sectoral aperture distribution for a rectangular array leads to an FW that is truncated at the array edges, plus FW-modulated diffracted contributions from the edges and vertexes of the array. The asymptotic results can be cast in the format of a generalized geometrical theory of diffraction (GTD) ray theory which includes periodicity-induced nonspecular reflections as well as multiple conical edge diffractions and spherical vertex diffractions. Since the FW series and the series of corresponding diffracted fields exhibit excellent convergence properties far enough away from the array plane to render evanescent FWs and diffracted fields negligible, the resulting representation is found to be more efficient than the direct summation over the spatial contributions from each element of the array.

This approach has been applied by us previously to semi-infinite planar dipole arrays [*Capolino et al.*, 2000a, b]; in the present paper we consider the

Paper number 1999RS900107.
0048-6604/00/1999RS900107$11.00

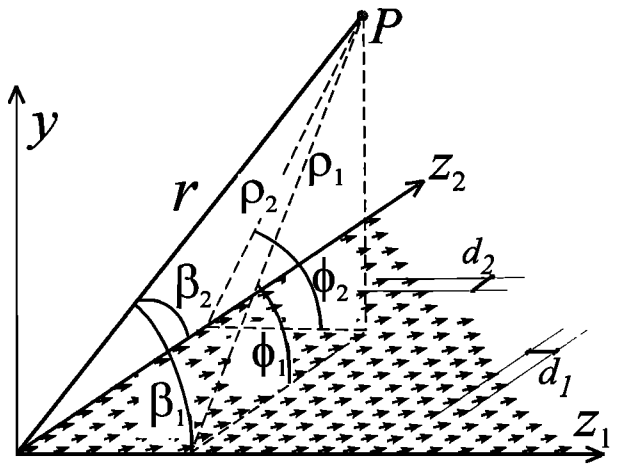

Figure 1. Geometry of the planar sectoral array of parallel dipoles oriented along a direction $\hat{u}$. Here d_1 and d_2 are the interelement spatial periods along z_1 and z_2, respectively.

problem of a right-angle sectoral planar phased dipole array, which combines the phenomenologies of the two truncated edges and includes the effect of vertex diffraction. The implementation is performed sequentially, initially treating the truncation effects due to the two edge arrays and thereafter including the effect of the vertex.

The sectoral AGF is constructed here by plane wave spectral decomposition in the two-dimensional wavenumber domain corresponding to the array-plane coordinates. The direct spectral summation over contributions from the individual radiators is restructured into a closed form with pole singularities, thereby yielding a double spectral integral for the radiated field. The analysis involves a sequence of manipulations in the complex two-dimensional spectral wavenumber plane that prepare the integrands for the subsequent efficient and physically incisive asymptotics, parameterized by critical spectral points (saddle point and poles). Different species of spectral poles define the various species of propagating and evanescent Floquet waves (FWs). The other critical points in the double spectral integral define the asymptotic behavior of the edge and vertex diffracted rays, and the confluence of these critical points determines a variety of locally uniform transition regions for truncated edge diffracted and vertex diffracted waves, for both propagating and evanescent FWs. To the best of our knowledge, our approach to the rigorous analysis and synthesis of the sectoral array Green's function in terms of self-consistent periodicity-modulated edge and vertex interactions is novel. Numerical examples verify the accuracy and efficiency of this asymptotics.

The canonical sectoral AGF here, which has linearly phased, uniform-amplitude dipoles, can be used as the basic constituent for structuring a full-wave analysis of actual rectangular arrays of short wire dipoles or of apertures in an infinite ground plane. The analysis can be carried out via the "windowing method" [*Ishimaru et al.*, 1985; *Skrivervik and Mosig*, 1992] or, more accurately, via the method of moments [*Neto et al.*, 1998; see also *Civi et al.*, 1998]. In each case, the canonical AGF is used in the integral equation for the actual array so as to isolate the noncanonical variations near the array edges and vertexes, thereby substantially reducing the numerical size of the overall problem. A more detailed description is given by *Maci et al.* [1999].

2. Formulation

The geometry of the infinite planar rectangular sector array of phased dipoles of unit current amplitude $\vec{J}$, located in the (z_1, z_2) plane, is shown in Figure 1; the arrow denotes a vector quantity. The interelement spatial period along the z_1 and z_2 directions is given by d_1 and d_2, respectively. All dipoles are oriented along the unit vector $\hat{u}$, and they are linearly phased with suppressed time dependence $\exp(j\omega t)$,

$$\vec{J}(md_1, nd_2) = \hat{u}e^{-j(\gamma_1 md_1 + \gamma_2 nd_2)}, \tag{1}$$

with $(z_1', z_2') \equiv (md_1, nd_2)$ denoting the position of dipole (m, n) and $\gamma_1/k = \cos\beta_1'$ and $\gamma_2/k = \cos\beta_2'$ denoting the interelement phase gradients expressed in terms of the direction cosines with respect to the (z_1, z_2) axes. The circumflex denotes a unit vector. The electromagnetic vector field at any observation point $\vec{r} = z_1\hat{z}_1 + z_2\hat{z}_2 + y\hat{y}$ can be derived from the magnetic vector potential

$$\vec{A}(\vec{r}) = \sum_{m=0}^{\infty}\sum_{n=0}^{\infty} g(\vec{r}; md_1, nd_2)\vec{J}(md_1, nd_2) \tag{2}$$

by summing over the individual dipole elements. In (2), g is the free-space scalar Green's function $g(\vec{r}; z_1', z_2') = \exp(-jk|\vec{R}|/(4\pi|\vec{R}|)$, with $\vec{R} = \vec{r} - z_1'\hat{z}_1 - z_2'\hat{z}_2$ and $\vec{r} = z_1\hat{z}_1 + z_2\hat{z}_2 + y\hat{y}$.

Our analysis is carried out in the spectral wavenum-

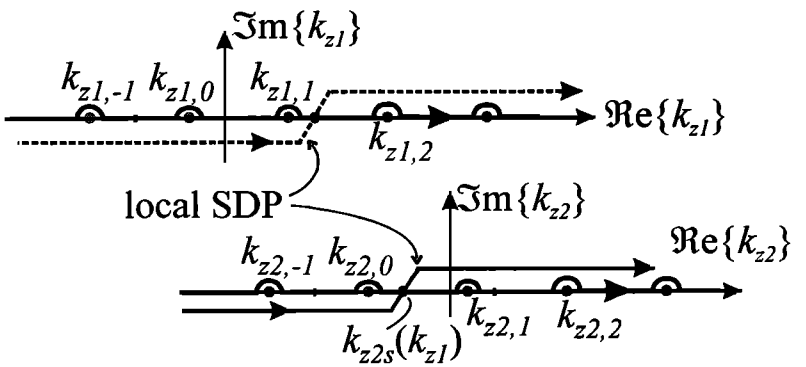

Figure 2. Topology of the k_{z1} and k_{z2} complex planes. The original integration paths of equations (5) and (10) are along the real axis with clockwise indentation around the poles. As described in section 3, the original integration paths are deformed locally along the 45°-line steepest-descent paths (SDPs). In the k_{z2} plane the SDP passes through the k_{z1}-dependent saddle point (SP) $k_{z2s}(k_{z1}) = \sqrt{k^2 - k_{z1}^2}\cos\phi_1$. Similarly, the local SDP in the k_{z1} plane passes through the SP $k_{z1s}(k_{z2}) = \sqrt{k^2 - k_{z2}^2}\cos\phi_2$.

ber domain. Accordingly, we employ the spectral Fourier representation [*Felsen and Marcuvitz*, 1973]

$$g(\vec{r}; z_1', z_2') = \frac{1}{8\pi^2 j}\int_{-\infty}^{\infty}\int_{-\infty}^{\infty}\frac{\exp(-j\vec{k}\cdot\vec{R})}{k_y}dk_{z1}\,dk_{z2}, \quad (3)$$

where

$$\vec{k} = k_{z1}\hat{z}_1 + k_{z2}\hat{z}_2 \pm k_y\hat{y}, \quad k_y = \sqrt{k^2 - k_{z1}^2 - k_{z2}^2} \quad (4)$$

and the upper and lower signs apply to $y > 0$ and $y < 0$, respectively. Because of the symmetry, from here on we shall deal with $y > 0$ only. On the top Riemann sheet of the complex k_{z1} plane, for real k_{z2}, we define $\mathrm{Im}(k_y) < 0$ for $k^2 - k_{z2}^2 < k_{z1}^2$ and $k_y > 0$ for $k^2 - k_{z2}^2 > k_{z1}^2$. The location of branch points and branch cuts with respect to the real-axis integration path in the k_{z1} plane is found by introducing small losses ($\mathrm{Im}(k) = 0^-$) which are eventually removed [*Capolino et al.*, 2000a]. Next, we substitute (3) into (2) and interchange the sequence of the m-sum and spectral integration operations, followed by summing the resulting m series into closed form. Because the spectral m-series summands are highly oscillatory undamped exponentials when k_{z1} is real, the m sum is ill-behaved. For stabilization, we introduce a small shift $\varepsilon > 0$ in the k_{z1} spectrum (note that $0 < \varepsilon < -\mathrm{Im}(k)$), thereby ensuring uniform convergence of the m sum along the displaced k_{z1} contour. The m sum has the closed form $\sum_{m=0}^{\infty}\exp(j(k_{z1} - \gamma_1)md_1) = [1 - \exp(jd_1(k_{z1} - \gamma_1)]^{-1}$, which has simple poles located at $k_{z1} = k_{z1,q}$ in (7). Letting $\varepsilon \to 0$ in the result leads to right (clockwise) indentation of the integration path around the k_{z1}-spectral poles (see Figure 2). Repeating the same steps for the n series and the k_{z2} integration leads to a closed form analogous to (6), with simple poles at $k_{z2,p}$ in (8). The vector potential is thereby expressed as

$$\vec{A}(\vec{r}) = \frac{\hat{u}}{8\pi^2 j} \cdot \int_{-\infty}^{\infty}\int_{-\infty}^{\infty}\frac{1}{k_y}B_1(k_{z1})B_2(k_{z2})\exp(-j\vec{k}\cdot\vec{r})\,dk_{z1}\,dk_{z2} \quad (5)$$

with the periodicity-induced closed-form spectral amplitudes

$$B_i(k_{zi}) = (1 - \exp(jd_i(k_{zi} - \gamma_i)))^{-1}, \quad i = 1, 2 \quad (6)$$

which have uncoupled q- and p-indexed poles in the (k_{z1}, k_{z2}) plane, located at

$$k_{z1,q} = \gamma_1 + \frac{2\pi q}{d_1}, \quad q = 0, \pm 1, \pm 2, \cdots \quad (7)$$

$$k_{z2,p} = \gamma_2 + \frac{2\pi p}{d_2}, \quad p = 0, \pm 1, \pm 2, \cdots. \quad (8)$$

These poles define the Floquet wave (FW) wavenumbers (i.e., the FW dispersion relations) along the z_1 and z_2 directions, respectively. The poles are located below the k_{z1}- and k_{z2}-integration paths in Figure 2, and their residues account collectively for the effects

of untruncated periodicity along the z_1 and z_2 coordinates, respectively.

It is convenient to introduce the FW propagation vector

$$\vec{k}_{pq}^{\,\mathrm{FW}} = k_{z1,q}\hat{z}_1 + k_{z2,p}\hat{z}_2 + k_{ypq}\hat{y}, \qquad k_{ypq} = \sqrt{k^2 - k_{z1,q}^2 - k_{z2,p}^2}. \tag{9}$$

For a propagating FW, $\vec{k}_{pq}^{\,\mathrm{PFW}}$ is real and identifies the radiation (ray) direction of the pqth propagating FW (FW_{pq}). For an evanescent FW, the y component of $\vec{k}_{pq}^{\,\mathrm{EFW}}$ (perpendicular to the array) is purely imaginary. The evanescent FWs propagate along the array plane with phase propagation (ray) vector $\mathrm{Re}(\vec{k}_{pq}^{\,\mathrm{EFW}})$, maintaining a phase speed less than the speed of light ($|\mathrm{Re}(\vec{k}_{pq}^{\,\mathrm{EFW}})| > k$), and exhibiting exponential decay along $|y|$ with attenuation vector $\mathrm{Im}(\vec{k}_{pq}^{\,\mathrm{EFW}}) = k_{ypq}\hat{y}$. The boundary between the propagating and evanescent FW regimes is defined by the cutoff condition $k_{ypq} = 0$.

The vector electric field is obtained from the vector potential $\vec{A}$ in (5) via $\vec{E} = -j\omega\mu(\vec{A} + \nabla\nabla\cdot\vec{A}/k^2)$, and the magnetic field is obtained via $\vec{H} = \nabla\times\vec{A}$. Interchanging the derivative and summation-integration operations and noting that the ∇ operator is transformed thereby into $(-j\vec{k})$ yields the compact expression

$$\vec{E}(\vec{r}) = \frac{1}{8\pi^2}\int_{-\infty}^{\infty}\int_{-\infty}^{\infty}(k_y)^{-1}B_1(k_{z1})B_2(k_{z2})\bar{\bar{G}}^E(\vec{k}) \cdot\hat{u}\exp(-j\vec{k}\cdot\vec{r})\,dk_{z1}\,dk_{z2}, \tag{10}$$

where $\bar{\bar{G}}^E(\vec{k}) = -\zeta/k(k^2\bar{\bar{I}} - \vec{k}\vec{k})$ is the dyadic electric field spectral Green's function, with $\bar{\bar{I}}$ denoting the unit dyadic, and the notation $\vec{k}$ in $\bar{\bar{G}}^E(\vec{k})$ implies a dependence on $(k_{z1}, k_{z2}, k_y(k_{z1}, k_{z2}))$. From here on we shall deal only with the electric field. The magnetic field is formally treated in similar fashion, leading to the replacement of $\bar{\bar{G}}^E(\vec{k})$ by the magnetic dyadic Green's function $\bar{\bar{G}}^H(\vec{k}) = -\vec{k}\times\bar{\bar{I}}$.

3. Solution Strategy: Synthesis via Canonical Constituents

As noted earlier, the residues at the two poles (k_{z1}, k_{z2}) in the integral (10) represent the FW_{pq} fields pertaining to the infinite periodic array. Explicitly, the electric field due to the infinite array is given by the FW series

$$\vec{E}_\infty = \sum_{p,q=-\infty}^{\infty}\vec{E}_{pq}^{\,\mathrm{FW}}(\vec{r}), \tag{11}$$

where

$$\vec{E}_{pq}^{\,\mathrm{FW}}(\vec{r}) = \bar{\bar{G}}^E(\vec{k}_{pq}^{\,\mathrm{FW}})\cdot\hat{u}\,\frac{\exp(-j\vec{k}_{pq}^{\,\mathrm{FW}}\cdot\vec{r})}{2d_1d_2k_{ypq}}. \tag{12}$$

The asymptotic evaluation of the integral in (10) shall be addressed sequentially, initially separating the truncation effects due to the two array edges along z_1 and z_2 from the effects of the vertex. Accordingly, we summarize first the results obtained by *Capolino et al.* [2000a, b] for radiation from a semi-infinite phased dipole array, and then account for the vertex effect in the sectoral array.

3.1. Semi-infinite Array With Edge Along the z_1 Axis

Referring to Figure 1, consider a semi-infinite array of dipoles with edge along z_1 (i.e., truncation along z_2) and dipole orientation vector $\hat{u}$. Contrasting this formulation with the one in section 2, we note the following differences:

1. Instead of (2), with (3), the semi-infinite array sums are $\sum_{m=-\infty}^{\infty}\sum_{n=0}^{\infty}$.
2. The resulting n series in the (k_{z2}) domain is summed into closed form as in (5).
3. The remaining m series in the spectral double integral is summed into closed form via the infinite Poisson sum formula,

$$\sum_{m=-\infty}^{\infty}\exp[j(k_{z1}-\gamma_1)d_1m] = \frac{2\pi}{d_1}\sum_{q=-\infty}^{\infty}\delta\left(k_{z1}-\gamma_1-\frac{2\pi q}{d_1}\right),$$

which reduces the k_{z1} integral to a q series. Instead of (10), we obtain the following exact solution:

$$\vec{E}_1(\vec{r}) = \frac{1}{4\pi d_1}\sum_{q=-\infty}^{\infty}e^{-jk_{z1,q}z_1}\vec{D}_2(k_{z1,q}) \tag{13a}$$

$$\vec{D}_2(k_{z1,q}) = \int_{-\infty}^{\infty}(k_{yq})^{-1}B_2(k_{z2})\bar{\bar{G}}^E(\vec{k}_q)\cdot\hat{u}e^{-j[k_{z2}z_2+k_{yq}y]}\,dk_{z2}, \tag{13b}$$

with $\vec{k}_q = k_{z1,q}\hat{z}_1 + k_{z2}\hat{z}_2 + k_{yq}\hat{y}$, where $k_{yq} = (k^2 - k_{z2}^2 - k_{z1,q}^2)^{-1/2}$, $k_{z1,q}$ is given in (7) and $B_2(k_{z2})$ is given in (6). Note that the infinite-edge field in (13) has a mixed integral-sum form, in which

partial (k_{z1}-domain) FW information is exhibited explicitly, while k_{z2}-domain FW information remains to be extracted by residue evaluation at the $k_{z2,p}$ poles in $\tilde{D}_2(k_{z1,q})$. In (10), for the sectoral configuration, the double spectral integral remains intact, and all the FW information remains to be extracted via the spectral poles. Equation (13) is in a form to which uniform saddle point–steepest descent techniques, as formalized by the *Van der Waerden* [1951] method for single integrals, can be applied directly. The method involves deformation of the original real-axis integration path into the steepest-descent path (SDP) (which can be approximated by the local SDP) through the saddle point of the phase in the integrand and extraction of the residues from intercepted poles. Application to (13b) leads to the following asymptotic result for the electric field $\tilde{\vec{E}}_1(\vec{r})$ radiated by the semi-infinite array [*Capolino et al.*, 2000a]:

$$\tilde{\vec{E}}_1(\vec{r}) = \sum_{p,q} U_{pq}^{\mathrm{FW},1} \tilde{\vec{E}}_{pq}^{\mathrm{FW}}(\vec{r}) + \sum_{q} \tilde{\vec{E}}_q^{d,1}(\vec{r}), \qquad (14)$$

where the first term, due to intercepted pole residues, yields a series of FWs $\tilde{\vec{E}}_{pq}^{\mathrm{FW}}(\vec{r})$ which are truncated versions of those defined in (12) for the infinite structure. The truncation function is simply

$$U_{pq}^{\mathrm{FW},1} = U(\phi_{1,pq}^{\mathrm{SB}} - \phi_1), \qquad (15)$$

where $U(\eta)$ is the Heaviside unit step function: $U(\eta) = 1$ for $\eta > 0$ and $U(\eta) = 0$ for $\eta < 0$; ϕ_1 is the transverse-to-z_1 observation angle (see Figure 1). The domain of existence of the FW_{pq} (the FW_{pq}-illuminated region) is thereby truncated at the shadow boundary planes $\phi_1 = \phi_{1,pq}^{\mathrm{SB}}$, where for propagating FWs

$$\phi_{1,pq}^{\mathrm{SB}} \equiv \phi_{1,pq} = \cos^{-1}\left(\frac{k_{z2,p}}{k_{\rho 1,q}}\right), \qquad (16a)$$

$$k_{\rho 1,q} = \sqrt{k^2 - k_{z1,q}^2}. \qquad (16b)$$

The $\phi_{1,pq}^{\mathrm{SB}}$ shadow boundary angle corresponds to the coincidence of the pq pole and the saddle point; the U function identifies the illuminated and shadowed sides (see Figure 3). The second term in (14), due to asymptotic evaluation of the SDP integral, yields a series of $\tilde{\vec{E}}_q^{d,1}$ fields which are q-indexed, p-independent FW-modulated edge-diffracted conical waves with respect to the array edge along the z_1 axis,

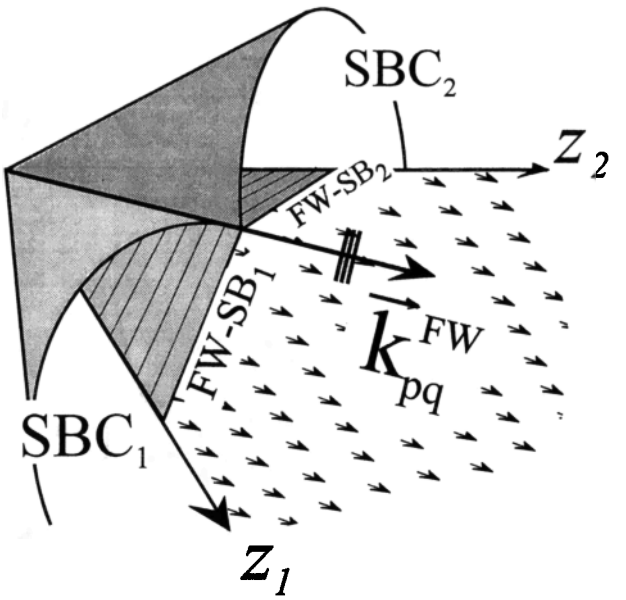

Figure 3. Geometry of the shadow boundaries (SBs). The Floquet wave (FW)-SB planes truncate the domain of existence of a FW with index pq. The truncated FW_{pq} exists under the "roof" formed by the intersection of the two FW-SBs. The diffracted rays $\tilde{\vec{E}}_q^{d,1}$ and $\tilde{\vec{E}}_p^{d,2}$ are truncated at the shadow boundary cones (SBC) with axes along edges 1 and 2. These two SBCs intersect along the intersection line of the two FW-SBs. This intersection line coincides with the propagation vector $\tilde{\vec{k}}_{pq}^{\mathrm{FW}}$ of the pq-FW.

$$\tilde{\vec{E}}_q^{d,1}(\vec{r}) \sim \frac{e^{-j\tilde{\vec{k}}_q^{d,1}\cdot\vec{r}}}{\sqrt{\rho_1}} \tilde{\vec{D}}_q^{d,1} \cdot \hat{u}. \qquad (17)$$

These waves, which are not affected by the z_2-domain p-indexed FW periodicity, provide the required continuity of the truncated FW fields across their shadow boundaries. The diffracted rays with wave vector $\tilde{\vec{k}}_q^{d,1}$

$$\tilde{\vec{k}}_q^{d,1} = k_{z1,q}\hat{z}_1 + k_{\rho 1,q}\cos\phi_1 \hat{z}_2 + k_{\rho 1,q}\sin\phi_1 \hat{y} \qquad (18)$$

reach the observer along diffraction cones with angle

$$\beta_{1,q} = \cos^{-1}(k_{z1,q}/k), \qquad |k_{z1,q}| < k \qquad (19)$$

(see Figure 4), which are FW-modulated generalizations of the smooth-edge version in conventional GTD. The uniform dyadic diffraction coefficient in (17) is

$$\tilde{\vec{D}}_q^{d,1} = \frac{\sqrt{j}}{2d_1\sqrt{2\pi k_{\rho 1,q}}}\left(B_2(k_{\rho 1,q}\cos\phi_1)\tilde{\vec{G}}^E(\tilde{\vec{k}}_q^{d,1}) + \sum_p \frac{\tilde{\vec{G}}^E(\tilde{\vec{k}}_{pq}^{\mathrm{FW}})[F(\delta_{1,pq}^2) - 1]}{jd_2 k_{\rho 1,q}(\cos\phi_{1,pq} - \cos\phi_1)}\right), \qquad (20)$$

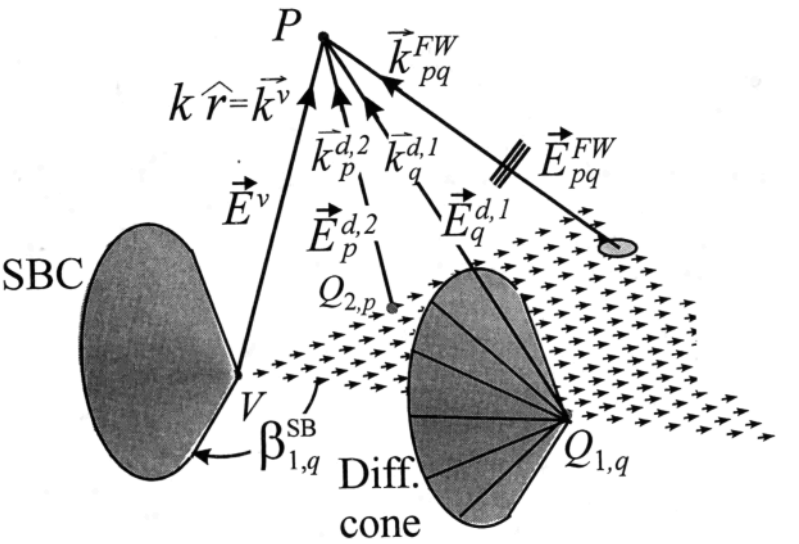

Figure 4. Ray description of the field radiated by the sectoral array of dipoles. The diffraction cone of the propagating z_1-edge diffracted field $\vec{E}^{d,1}_q$ originates at the q-dependent point $Q_{1,q}$ on edge 1. The SBC that truncates the domain of existence of $\vec{E}^{d,1}_q$ has the same aperture angle $\beta_{1,q}$ as the diffraction cone, and it is centered at the vertex.

where

$$\delta_{1,pq} = \sqrt{2k_{\rho 1,q}\rho_1}\,\sin\left[\tfrac{1}{2}(\phi_{1,pq} - \phi_1)\right] \qquad (21)$$

and F denotes the transition function of the uniform theory of diffraction (UTD) [*Kouyoumjian and Pathak*, 1974],

$$F(x) = 2j\sqrt{x}e^{jx}\int_{\sqrt{x}}^{\infty} e^{-jt^2}\,dt, \quad -\frac{3\pi}{2} < \arg(x) \le \frac{\pi}{2}. \qquad (22)$$

Concerning the uniform asymptotic edge diffracted field, the Van der Waerden method, by adding and subtracting regularizing portions of the integrand, can account systematically and uniformly for any number of spectral poles in the SDP integral [see *Capolino et al.*, 2000a]. In practice, one employs the regularization only for those poles which are "sufficiently close" to the saddle point to affect the isolated saddle point approximation. The procedure applies to both propagating FW and evanescent FW pole contributions and yields the uniform transition functions across the shadow boundaries of these FWs. Equation (17) with (20) is a simplified version, in which only the propagating FW poles are regularized in the asymptotic process. This yields a more convenient, but still accurate, high-frequency algorithm. It is demonstrated by *Capolino et al.* [2000a] that the contribution from the uniform treatment of evanescent FW is nonnegligible only in a few special cases.

The function F in (22) tends to unity for "large" amplitude of its argument $\delta_{1,pq}$, i.e., for observation points "far" from the shadow boundary planes. In the same observation range the quantity $(1 - F)$ is of asymptotic order $(k_{\rho q}\rho)^{-1}$, so that the dominant asymptotic contribution to the diffraction coefficient is $B_2(k_{\rho 1,q}\cos\phi_1)\bar{\bar{G}}^E(\vec{k}^{d,1}_q)$ in (20), which characterizes the nonuniform edge diffraction field. Thus the "large $\delta_{1,pq}$" range connects the transition function in the second term of (20) smoothly with the nonuniform first term in an overlapping region. Note that large $\delta_{1,pq}$ can be reached (1) by specifying $\phi_{1,pq} \approx \phi_1$ and/or ρ_1 small with large enough k, or (2) by specifying k with large enough $(\phi_{1,pq} - \phi_1)$ and/or ρ_1. This type of asymptotic "patching" will be utilized repeatedly later on.

When $|k_{z1,q}| > k$, the resulting diffracted field is evanescent along the ρ_1 direction, with exponential decay term $\exp(-|k_{\rho 1,q}|\rho_1)$, since in this case $k_{\rho 1,q} = -j|k_{\rho 1,q}|$ (see equation (17)). The radially attenuated diffracted waves are negligible even relatively close to the edge, and the q series of diffracted rays in (14) may be truncated in such a way as to include only propagating diffracted waves (those with $|k_{z1,q}| < k$). This renders the FW formulation substantially more

efficient than element-by-element summation. Referring to Figure 1, the treatment of the semi-infinite array with edge along z_2 proceeds like that above, with interchange of indexes 1 and 2 and indexes q and p.

3.2. Planar Sectoral Array

The exact solution in (5) or (10) for the sectoral array in Figure 1 combines the phenomenologies of the two semi-infinite arrays in section 3.1 with that of the vertex. Note that via the Van der Waerden–(steepest descent path) procedure, each single integral, as represented in (13b) or its z_2-edge analog, contributes two terms arising from the intercepted poles and SDP integration, respectively. Poles essentially define truncated FWs, and saddle point asymptotics defines conical edge diffractions. Via the double (k_{z1}, k_{z2}) integration in (10), to be performed sequentially in this section so as to match the format in (13a) and (13b) (see equations (25a) and (25b)), the semi-infinite array FW and edge-diffracted phenomenologies become intertwined and yield a rich variety of interacting wave processes.

The behavior of the exact solution is parameterized by the critical points in the spectral double integral, which also govern the strategies for asymptotic approximations. The critical points in (5) or (10) are

First-order (k_{z1}, k_{z2})-saddle point $(\bar{k}_{z1s}, \bar{k}_{z2s})$

$$(d/dk_{zi})(\vec{k}\cdot\vec{r})_s = 0,\ i = 1, 2,\quad |\det(d^2/dk_{zi}dk_{zj})(\vec{k}\cdot\vec{r})_s| \neq 0$$

k_{z1} poles $\quad k_{z1,q}$ in equation (7) (23)

k_{z2} poles $\quad k_{z2,p}$ in equation (8)

In (23), $|\det(d^2/dk_{zi}dk_{zj})(\vec{k}\cdot\vec{r})_s|$ is the Hessian determinant.

For the semi-infinite array solution in (17) with edge along the z_1 axis, the critical points of the integration domain in (13a) are

k_{z2}-saddle point $k_{z2s}(k_{z1,q})$ $\quad \dfrac{d}{dk_{z2}}(\vec{k}\cdot\vec{r})_s = 0$ (24)

k_{z2} poles $\quad k_{z2,p}$ in equation (8)

In (13a) and (13b) the $k_{z1,q}$ footprint of the z_1 periodicity is embedded in the k_{z2} integral via the wavenumber k_{yq}, whereas in (10) the k_{z2} phase is not restricted and the z_1-periodicity footprint is embedded within the k_{z1} poles in (7). For the semi-infinite array with edge along the z_2 axis, the analogous critical points are as in (24), with k_{z1} replaced by k_{z2} and $k_{z1,q}$ replaced by $k_{z2,p}$. We therefore observe that the principal difference in critical point configurations between the sectoral and the two constituent semi-infinite array configurations is the two-dimensional saddle point for the sector versus the one-dimensional saddle point for each edge (without vertex).

3.2.1. Determination of the FW shadow boundaries. Rewriting the double integration in (10) sequentially yields

$$\tilde{E}(\vec{r}) = \frac{1}{8\pi^2}\int_{-\infty}^{\infty} dk_{z1}e^{-jk_{z1}z_1}B_1(k_{z1})\tilde{D}_2(k_{z1})\,dk_{z1} \quad (25a)$$

$$\tilde{D}_2(k_{z1}) = \int_{-\infty}^{\infty}(k_y)^{-1}B_2(k_{z2})\bar{\bar{G}}^E(\vec{k})\cdot\hat{u}e^{-j[k_{z2}z_2+k_yy]}\,dk_{z2}. \quad (25b)$$

The field structure of the sectoral array in (25a) and (25b) differs from that of the semi-infinite array in (13) with respect to the k_{z1} integration which replaces the k_{z1} summation in (13a). This difference results from the fact that the sectoral array field is aperiodic due to truncation also along z_1. Note that the residues of (25a) at the spectral poles $k_{z1,q}$ of $B_1(k_{z1})$ yield exactly the field (13a) of the semi-infinite array with edge along z_1, while the k_{z2} poles of (25b) incorporate the FW phenomenology associated with the infinite-edge configuration along z_2. Furthermore, for certain observation regions "far away" from the apex, it can be anticipated that the FW_{pq} shadow boundary planes pertaining to the sectoral array are given by $\phi^{\mathrm{SB}}_{1,pq}$ in (16a) with respect to edge z_1 and by the analogous $\phi^{\mathrm{SB}}_{2,pq} = \cos^{-1}(k_{z1,q}/k_{\rho 2,p})$, $k_{\rho 2,p} = \sqrt{k^2 - k^2_{z2,p}}$, with respect to edge z_2 (see section 3.2). To verify this conjecture, we transform from the rectilinear space and k_{z2}-spectrum variables pertaining to $\tilde{D}_2$ in (25b) to cylindrical spatial and angular spectral coordinates: $z_2 = \rho_1\cos\phi_1$, $y = \rho_1\sin\phi_1$, $k_{z2} = k_{\rho 1}\cos\alpha_1$, and $k_y = k_{\rho 1}\sin\alpha_1$, with $k_{\rho 1} = \sqrt{k^2 - k^2_{z1}}$. Note that $k_{\rho 1}$ has a functional dependence on the external variable of integration k_{z1} which is not always explicitly indicated. The phase in the integrand of $\tilde{D}$ is written as $k_{z2}z_2 + k_y y = k_{\rho 1}\rho_1\cos(\alpha_1 - \phi_1)$, which has a saddle point at $\alpha_{1s} = \phi_1$, corresponding to the k_{z1}-dependent saddle point $k_{z2s}(k_{z1})$ in the original spectral variable k_{z2}: $k_{z2s}(k_{z1}) = \sqrt{k^2 - k^2_{z1}}\cos\phi_1$. To gain information about FW shadow boundaries associated with edge 1 and 2, respectively (see discussion pertaining to

(13b)), it is necessary to traverse along the SDP locally into the complex wavenumber plane. Applying the single-edge spectral strategy to the sectoral solution in (10) is complicated by the fact that the saddle point and the SDP must be tracked in two complex planes (k_{z1}, k_{z2}) simultaneously. To deal with this problem, remaining cognizant of the constituent semi-infinite array solutions, the original integration path is deformed locally into the complex k_{z2} SDP (Figure 2) along the 45° line through the saddle point. Any poles $k_{z2,p}$ intercepted during the deformation contribute k_{z1}-dependent residues $\tilde{R}_2(k_{z1})$ which need to be included. This leads to

$$\tilde{E}(\vec{r}) = \tilde{E}_S(\vec{r}) + \tilde{E}_R(\vec{r}) = \frac{1}{8\pi^2}\int_{-\infty}^{\infty} dk_{z1} e^{-jk_{z1}z_1} B_1(k_{z1}) \cdot [\tilde{D}_2(k_{z1})_{\mathrm{SDP}} + 2\pi j \tilde{R}_2(k_{z1})], \quad (26)$$

where $\tilde{E}_S$ corresponds to the contribution from the first term in the integrand, i.e., from $\tilde{D}_2(k_{z1})_{\mathrm{SDP}}$ in (25b) along the local SDP integration path. The residue-induced contribution $\tilde{E}_R$ corresponds to the second term in the integrand,

$$\tilde{R}_2(k_{z1}) = \sum_{p=-\infty}^{\infty} U[k_{z2s}(k_{z1}) - k_{z2,p}] \cdot (jd_2 k_{yp})^{-1} \tilde{G}^E(\vec{k}_p) \cdot \hat{u} e^{-j[k_{z2,p}z_2 + k_{yp}y]}, \quad (27)$$

with $\vec{k}_p = k_{z1}\hat{z}_1 + k_{z2,p}\hat{z}_2 + k_{yp}\hat{y}$, where $k_{yp} = (k^2 - k_{z1}^2 - k_{z2,p}^2)^{-1/2}$. Note that the $\tilde{E}_R(\vec{r})$ portion in (26) is formally equal to (13) except for the interchange of 1 and 2 and of q and p, and of the presence of the truncation function $U[k_{z2s}(k_{z1}) - k_{z2,p}]$ in (27) in the integrand of (26).

To complete the FW shadow boundary identification, we change variables in $\tilde{E}_R(\vec{r})$ of (26) to $k_{z1} = k_{\rho 2,p}\cos\alpha_2$, $k_{yq} = k_{\rho 2,p}\sin\alpha_2$, where $k_{\rho 2,p} = \sqrt{k^2 - k_{z2,p}^2}$, and also $z_1 = \rho_2\cos\phi_2, y = \rho_2\sin\phi_2$, so that the k_{z1}-dependent phase function in (27) becomes $[k_{z1}z_1 + k_{yq}y] = k_{\rho 2,p}\rho_2\cos(\alpha_2 - \phi_2)$. Therefore the saddle point is located at $\alpha_{2s} = \phi_2$, which corresponds to $k_{z1} = k_{z1s}(k_{z2,p}) = k_{\rho 2,p}\cos\phi_2$. The k_{z1}-integration path is now deformed into the local SDP($k_{z1s}(k_{z2,p})$), and any poles $k_{z1} = k_{z1,q}$ intercepted during the deformation are extracted to yield $\tilde{E}_R(\vec{r}) = \tilde{E}_R^{\mathrm{FW}}(\vec{r}) + \tilde{E}^{d,2}(\vec{r})$, where $\tilde{E}^{d,2}(\vec{r})$ corresponds to the local SDP integration and $\tilde{E}_R^{\mathrm{FW}}(\vec{r})$ corresponds to the residues:

$$\tilde{E}_R^{\mathrm{FW}}(\vec{r}) = \sum_{q=-\infty}^{\infty}\sum_{p=-\infty}^{\infty} \tilde{E}_{pq}^{\mathrm{FW}} U_{pq}^{\mathrm{FW},1} U_{pq}^{\mathrm{FW},2} \quad (28)$$

with $\tilde{E}_{pq}^{\mathrm{FW}}$ and $U_{pq}^{\mathrm{FW},1}$ given by (12) and (15) and $U_{pq}^{\mathrm{FW},2} = U(\phi_{2,pq} - \phi_2)$. The result in (28) represents sums of FW_{pq} fields on the infinite array (see equations (11) and (12)), truncated via the two U functions along shadow boundaries which conform with those pertaining to the infinite z_1-edge and z_2-edge cases, respectively. This confirms the conjecture made earlier and, via the above derivation, gives it a rigorous foundation.

3.2.2. Determination of the edge–diffracted wave shadow boundaries. The first term $\tilde{E}_S(\vec{r})$ in (26) may again be treated by contour deformation into the local 45°-line SDP through the saddle point $k_{z1s}(k_{z2}) = k_{\rho 2}\cos\phi_2 = \sqrt{k^2 - k_{z2}^2}\cos\phi_2$ (Figure 2), with extraction of residues due to intercepted $k_{z1,q}$ poles. Thus $\tilde{E}_S(\vec{r}) = \tilde{E}^{d,1}(\vec{r}) + \tilde{E}^{v}(\vec{r})$, where the first and second terms correspond to the sum of residues and to the SDP integration, respectively. The sectoral array field has thereby been restructured into the exact representation (i.e., before performing asymptotics)

$$\tilde{E}(\vec{r}) = \tilde{E}_R^{\mathrm{FW}}(\vec{r}) + \tilde{E}^{d,1}(\vec{r}) + \tilde{E}^{d,2}(\vec{r}) + \tilde{E}^{v}(\vec{r}), \quad (29)$$

where $\tilde{E}_R^{\mathrm{FW}}(\vec{r})$ is defined in (28). The field $\tilde{E}^{d,1}(\vec{r})$ is identical to the semi-infinite array field in (13a) and (13b), but evaluated along the local SDP (Figure 2), and with the truncation function $U[k_{z1s}(k_{z2}) - k_{z1,q}]$ included in the integrand; the field $\tilde{E}_2^d(\vec{r})$ is obtained from $\tilde{E}_1^d(\vec{r})$ by interchanging the indexes 1 and 2. The field $\tilde{E}^{v}(\vec{r})$ is given by the integral in (10), but with local SDP integration contours through the $(\bar{k}_{z1s}, \bar{k}_{z2s})$ saddle point in both variables (see Figure 2). The two terms $\tilde{E}^{d,1}(\vec{r})$ and $\tilde{E}^{d,2}(\vec{r})$ represent the diffraction contributions from edge 1 and edge 2, respectively, which include truncation effects at the vertex, while $\tilde{E}^{v}(\vec{r})$ is the vertex diffracted field. The z_1-edge integral can be evaluated asymptotically at the saddle point $k_{z2s}(k_{z1,q}) = k_{\rho 1,q}\cos\phi_1$, thus leading to the same edge-diffracted ray fields $\tilde{E}_q^{d,1}(\vec{r})$ as in (17)–(20) but multiplied by the truncation function

$$U[k_{z1s}(k_{z2s}(k_{z1,q})) - k_{z1,q}] = U(\beta_{1,q}^{\mathrm{SB}} - \beta_1) \equiv U_q^{d,1}, \quad (30)$$

where $\beta_{1,q}^{\mathrm{SB}} \equiv \beta_{1,q}$ is the shadow boundary cone ($\mathrm{SBC}_{1,q}$) angle given in (19). The $\mathrm{SBC}_{1,q}$ has the same aperture as the diffraction cone (19), but it is

centered at the vertex (Figure 4). The SBC truncates the domain of existence of the z_1-edge diffracted waves. Analogous considerations apply to the p-indexed, q-independent z_2-edge diffracted rays, whose domain of existence is confined to $U[k_{z2s}(k_{z1s}(k_{z2,p})) - k_{z2,p}] = U(\beta_{2,p}^{SB} - \beta_2) = U_p^{d,2}$.

3.2.3. Transition regions. So far, we have obtained the following expression for the sectoral array field:

$$\tilde{E}(\vec{r}) = \sum_{p,q} U_{pq}^{FW,1} U_{pq}^{FW,2} \tilde{E}_{pq}^{FW}(\vec{r}) + \sum_{q} U_q^{d,1} \tilde{E}_q^{d,1}(\vec{r}) + \sum_{p} U_p^{d,2} \tilde{E}_p^{d,2}(\vec{r}) + \tilde{E}^{v}(\vec{r}), \quad (31)$$

where $U_{pq}^{FW,1}$ is defined in (15), $U_q^{d,1}$ is defined in (30), and $\tilde{E}_q^{d,1}(\vec{r})$ is defined in (17) and (20). In the vicinity of the shadow boundary of any FW or edge-diffracted wave species, nonuniform asymptotics generally becomes inapplicable. Uniform asymptotic methods must be invoked there in order to ensure smooth compensation of the abrupt emergence or disappearence of any particular wave species across its shadow boundary. The (FW-shadow boundary)–(edge-diffracted) compensation mechanism away from the vertex is contained in the uniform diffracted field in (20), as discussed in detail in section 3.1. Near the vertex the z_1-edge and z_2-edge FW–shadow boundary transitions in sections 3.1 and 3.2 interact with the vertex-induced SBCs centered on the z_1 and z_2 axes, respectively, due to the truncation of the corresponding edge diffracted fields (Figures 3 and 4). The confluence of these four shadow boundary transitions near the vertex defines the asymptotics pertaining to vertex diffraction. The successive decompositions of the double spectral integral solutions over real (k_{z1}, k_{z2}) wavenumbers in (10) into integrations along complex (k_{z1}, k_{z2}) SDPs, with concomitant extraction of intercepted pole residues, provides the rigorous framework for asymptotic evaluation. These decompositions, which are exact before performing SDP asymptotics, have been summarized in (25)–(31). Developing the uniform asymptotics pertaining to the vertex, and reducing the resulting transition function to the simpler uniform expressions in section 3.1 away from the vertex, is beyond the scope of this paper and will be addressed separately (F. Capolino et al., manuscript in preparation, 1999). However, the framework for the Van der Waerden asymptotics and its lowest-order implementation is presented in section 4.

4. Canonical Integral for Vertex Diffraction

Within the Van der Waerden method the asymptotic evaluation of integrals characterized by specific arrangements of critical parameters (saddle points and singularities) is addressed by mapping the given integrand (both phase and amplitude) onto the simplest canonical integrand that accommodates the relevant configuration of critical points. The reduction to the canonical form is accomplished by selectively adding and subtracting "regularizing" portions of the integrand, which can involve an arbitrary number of poles; for simplicity here, we develop expressions only for regularization of the (p, q) pole which is closest to the saddle point. For the vertex problem the critical parameters are tied to the (k_{z1}, k_{z2}) first-order saddle point in (23) and to the k_{z1} and k_{z2} poles in (23). We shall be satisfied here with the lowest-order, locally uniform canonical asymptotics that extends over a limited region Q in the (k_{z1}, k_{z2}) spectral domain, large enough to accommodate the asymptotic isolation of the saddle point and poles at its boundary, and with its center defined by saddle point–pole coalescence. In section 4.1 we consider the proposed regularization architecture, and in section 4.2 we deal with the relevant asymptotics.

4.1. Spectral Regularization

The spectral regularizations pertaining to the vertex are summarized in Tables 1 and 2, which we now explain. Starting in Table 1 with the spectral amplitude in the integrand of (10), we refer to the discussion in section 3 on parameterizing the uniform sectoral array asymptotics in terms of the interaction, via the vertex, of the uniform semi-infinite array solutions pertaining to each edge. These phenomenologies are identified in the leftmost column, beginning sequentially with edge 1. The second column identifies the relevant spectral amplitude terms, while the third and fourth columns specify the corresponding critical spectral parameters. Note that $B_{1,2}$ contains the pole singularities in the $k_{z1,2}$ integrations, respectively (see equations (6)–(8)). The rightmost column gives the Van der Waerden regularization which isolates, via the $W_{1,q}$ and $W_{2,p}$ functions, the effect of the (p, q) poles under consideration. Note that $B_i(k_{zi}) = 1/2 + \sum_{\xi=-\infty}^{\infty} W_{i,\xi}$, where $W_{i,\xi} = [-jd_i(k_{zi} - k_{zi,\xi})]^{-1}$, with $\xi = q$ or p for $i = 1$ or

Table 1. Van der Waerden Regularization of the Spectral Integrand in Equation (10): $S \equiv B_1 B_2 G(k)$

Constituent Phenomenology	Relevant Spectral Coefficients	Poles	Constraint	Regularization
Edge-1 effect (k_{z2} integral (see equation (17b))	$B_2G(k)$	$k_{z2,p}$	$k_{z1} = k_{z1,q}$	$(B_2G(k) - W_{2,p}G(k_p)) + W_{2,p}G(k_p)$
Edge-2 effect on edge 1 (k_{z1} integral)	$B_1[B_2G(k)] = B_2[B_1G(k)] = \sum_{i=0}^{3} S_i$	$k_{z1,q}$	$k_{z2} = k_{z2,p}$	$B_2[(B_1G(k) - W_{1,q}G(k_q)) + W_{1,q}G(k_q)] - W_{2,p}[(B_1G(k_p) - W_{1,q}G(k_{pq})) + W_{1,q}G(k_{pq})] + W_{2,p}[(B_1G(k_p) - W_{1,q}G(k_{pq})) + W_{1,q}G(k_{pq})]$

In Tables 1 and 2, $k \to \vec{k}$ in equation (4); $k_{pq} \to \vec{k}_{pq}^{FW}$ in equation (9); $k^v \to \vec{k}^v = \bar{k}_{z1s}\hat{z}_1 + \bar{k}_{z2s}\hat{z}_2 + (k^2 - \bar{k}_{z1s}^2 - \bar{k}_{z2s}^2)^{1/2}\hat{y}$, with $\bar{k}_{zis} = k \cos \beta_i$; $B_{1,2} \to B_{1,2}(k_{z1,2})$ in equation (6); $G(k) \to \bar{\bar{G}}^E(\vec{k})$; $W_{1,q} = [-jd_1(k_{z1} - k_{z1,q})]^{-1}$; $W_{2,p} = [-jd_2(k_{z2} - k_{z2,p})]^{-1}$; and $S_i \to \bar{\bar{S}}_i(k_{z1}, k_{z2})$.

2, respectively. The pole singularities in $B_i(k_{zi})$ correspond to both propagating and evanescent FWs. Using this representation, the regular remainder functions with respect to a particular propagating FW pole are directly expressed as sums of the terms $W_{i,\xi}$ associated with the remaining propagating FW poles and evanescent FW poles.

While the pole extraction is direct for edge 1, the corresponding treatment of edge 2 is more involved because it is preconditioned by the presence of edge 1. Altogether, the regularization of $\bar{\bar{S}}(k_{z1}, k_{z2})$ leads to the nine individual terms in Table 1, which are rearranged in the rightmost column of Table 2 into four groups: $\bar{\bar{S}}_i(k_{z1}, k_{z2})$, $i = 0, \cdots, 3$. Each group addresses uniform transition through a critical spatial domain listed in the leftmost column, with the relevant critical parameters listed in the second column. Note that these regularizing decompositions are exact for the propagating FW spectrum (evanescent effects are neglected here), and they provide the formal structure for subsequent uniform asymptotics. The detailed blending of these complex vertex-induced phenomena with one another and with those exterior to the vertex region will be addressed elsewhere (F. Capolino et al., manuscript in preparation, 1999). For the present discussion we shall be satisfied with the lowest-order locally uniform asymptotic evaluation performed next.

4.2. Asymptotic Evaluation

The spectral decomposition in Table 2 leads to the exact spatial representation of the vertex diffracted field contribution,

$$\vec{E}^v(\vec{r}) = \vec{E}_0^v + \vec{E}_1^v + \vec{E}_2^v + \vec{E}_3^v, \tag{32}$$

where $\vec{E}_i^v$ $(i = 0, \cdots, 3)$ involves the spectral integrand $(8\pi^2 k_y)^{-1}\bar{\bar{S}}_i(k_{z1}, k_{z2}) \cdot \hat{u}e^{-j\vec{k}\cdot\vec{r}}$ and the (k_{z1}, k_{z2}) integration is performed near the real k_{z1}, k_{z2} axes along the local SDPs (Figure 2). The asymptotics of $\vec{E}_i^v$ is dominated by the value of the integrands at the saddle point $(k_{z1}, k_{z2}) \equiv (\bar{k}_{z1s}, \bar{k}_{z2s}) \equiv (k \cos \beta_1, k \cos \beta_2)$, as determined from (23) for the phase $\vec{k} \cdot \vec{r}$. Accordingly, in (23), $\vec{k}^v = \bar{k}_{z1s}\hat{z}_1 + \bar{k}_{z2s}\hat{z}_2 + (k^2 - \bar{k}_{z1s}^2 - \bar{k}_{z2s}^2)^{1/2}\hat{y} = k\hat{r}$, and the saddle point phase is kr. Taylor expansion of the phase up to second order around the saddle point gives

$$\vec{k}\cdot\vec{r} \approx kr - (A(k_{z1} - \bar{k}_{z1s})^2 + 2H(k_{z1} - \bar{k}_{z1s})(k_{z2} - \bar{k}_{z2s}) + B(k_{z2} - \bar{k}_{z2s})^2), \tag{33}$$

with coefficients $A = kr/(2k^2 \sin^2 \phi_2)$, $B = kr/(2k^2 \sin^2 \phi_1)$, and $H = kr \cos \beta_2 \cos \beta_1/(2k^2 \sin^2 \beta_2 \sin^2 \phi_2)$. Use has been made here of the conversion from the $k_{z1,2}$ variables to the angular variables as in the text following (25). This quadratic form is the lowest-

Table 2. Canonical Vertex Regularizations

Phenomenology (Transition Regions, Figure 3)	Critical Parameters	Regularized Coefficient
Near intersection of SB_1 and SB_2	$k^v \approx k_{pq}$	$S_0 = G(k_{pq})W_{1,q}W_{2,p}$
Near SBC_1	$\bar{k}_{z1s} \approx k_{z1,q}$	$S_1 = W_{1,q}[B_2G(k_q) - W_{2,p}G(k_{pq})]$
Near SBC_2	$\bar{k}_{z2s} \approx k_{z2,p}$	$S_2 = W_{2,p}[B_1G(k_p) - W_{1,q}G(k_{pq})]$
Near the vertex	$\bar{k}_{z1s}, \bar{k}_{z2s}$	$S_3 = S - \sum_{i=0}^{2} S_i$

SBC, shadow boundary cone.

order approximation to the exact phase over a limited region Q centered at the saddle point in the (k_{z1}, k_{z2}) domain, which is "sufficiently large" to uniformly accommodate the poles in the various spectral terms $\bar{\bar{S}}_i(k_{z1}, k_{z2})$ in Table 2. Since the $\vec{E}_0^v$ integral is the only one that has two poles (one in each variable), its asymptotic evaluation is carried out first. The other integrals can be asymptotically evaluated by reduction of $\vec{E}_0^v$.

The asymptotic evaluation of $\vec{E}_0^v$ is performed successively. First, we change variables to $\xi = \sqrt{A}(\bar{k}_{z1s} - k_{z1})$ and $\eta = \sqrt{B}(\bar{k}_{z2s} - k_{z2})$ to transform the quadratic phase in (33) into $\vec{k} \cdot \vec{r} \approx kr - (\xi^2 + 2w\xi\eta + \eta^2)$, with

$$w = H/\sqrt{AB} = \cot \beta_1 \cot \beta_2 = \cos \phi_1 \cos \phi_2. \tag{34}$$

Next, the regular slowly varying amplitude function $\bar{\bar{G}}^E(\vec{k}_{pq}^{FW}) \cdot \hat{u}(8\pi^2 k_y)^{-1}$ in the integrand (see Table 2 for S_0) is evaluated at the saddle point $(\xi, \eta) = (0, 0)$ and removed from the integral, with the result $\vec{E}_0^v \sim \bar{\bar{S}}_0(\bar{k}_{z1s}, \bar{k}_{z2s}) \cdot \hat{u} e^{-jkr} j(8\pi k_{ys}\sqrt{AB - H^2})^{-1} T(a_q, b_p, w)$, where

$$T(a_q, b_p, w) = \frac{a_q b_p}{j\pi\sqrt{1-w^2}} \cdot \int_{-\infty}^{\infty}\int_{-\infty}^{\infty} \frac{e^{j(\xi^2 + 2w\xi\eta + \eta^2)}}{\left(\xi - \dfrac{a_q}{\sqrt{1-w^2}}\right)\left(\eta - \dfrac{b_p}{\sqrt{1-w^2}}\right)} d\xi\, d\eta \tag{35}$$

and $a_q = \sqrt{A(1-w^2)}\,(\bar{k}_{z1s} - k_{z1,q})$ and $b_p = \sqrt{B(1-w^2)}\,(\bar{k}_{z2s} - k_{z2,p})$. Note that the (ξ, η) integral in (35) is actually the canonical mapping, in the rigorous Van der Waerden method, from the original (k_{z1}, k_{z2}) integral onto the simplest spectral integrand that accommodates a two-dimensional (2-D) first-order saddle point and a simple pole in each variable. Here, however, we have merely expanded the original phase directly to second order. A related approach was introduced by *Hill* [1990] and used by *Capolino and Maci* [1996]. The approach by *Hill* [1990] involves a more complicated pole-dependent mapping of the phase in (10) onto a quadratic canonical form similar to that in (33). Our procedure is more direct and, as we have found, quite accurate (see section 5). The normalization constant in (35) is such that $T(a, b, w)$ tends to unity for large values of the parameters a and b (i.e., for poles far from the saddle point). The numerical evaluation of (35) can be performed as by *Capolino and Maci* [1995], *Capolino et al.* [1997], and *Albani et al.* [1997] in terms of standard generalized Fresnel integrals [*Jones*, 1971]. It should be noted that in the transition regime where the poles are close to the saddle point, a_q and b_p can be approximated up to second order by the simpler expressions

$$a_q \approx \sqrt{2kr} \sin\left(\frac{\beta_{1,q} - \beta_1}{2}\right); \tag{36a}$$

$$b_p \approx \sqrt{2kr} \sin\left(\frac{\beta_{2,p} - \beta_2}{2}\right). \tag{36b}$$

Large values of a_q and b_p, away from the saddle point, define the nonuniform regime where $T \to 1$. This criterion defines the extent of the local region Q mentioned at the beginning of this section, which permits patching onto the nonuniform asymptotics exterior to Q. Since the expressions in (36a) and (36b) parameterize the single-edge diffractions in section 3 (recall equation (21)), we retain them throughout the exterior of Q (see remarks at the end of section 3.1). Via this strategy the function T in (35) yields the canonical UTD transition function when one of the two poles is asymptotically far from the saddle point since $T(a_q, |b_p| \gg 1, w) \sim F(a_q^2)$, $T(|a_q| \gg 1, b_p, w) \sim F(b_p^2)$, where $F(x)$ is defined in (22). The $|b_p| \gg 1$ limit may be obtained directly from (35) by approximating $(\eta - b_p/\sqrt{1-w^2})^{-1} \approx -b_p^{-1}\sqrt{1-w^2}$ in (35) and recognizing that the remaining single-pole integral is an ordinary UTD transition function. Therefore the reduced forms of (35) lead directly to the single pole integrals appearing in $\vec{E}_1^v$ and $\vec{E}_2^v$ in (32), respectively. The term $\vec{E}_3^v$ is evaluated asymptotically in a straightforward manner since $\bar{\bar{S}}_3$ is regular in the region Q. Finally, observing that $k_{ys}\sqrt{AB - H^2} = r/2$, we obtain

$$\vec{E}_i^v \sim \bar{\bar{S}}_i(\bar{k}_{z1s}, \bar{k}_{z2s}) \cdot \hat{u} \frac{je^{-jkr}}{4\pi r} \mathcal{T}_i, \qquad i = 0, \cdots, 3, \tag{37}$$

where $\mathcal{T}_0 = T(a_q, b_p, w)$, $\mathcal{T}_1 = F(a_q^2)$, $\mathcal{T}_2 = F(b_p^2)$, and $\mathcal{T}_3 = 1$, with $\bar{\bar{S}}_i$ identified in Table 2.

4.3. Vertex Diffracted Ray

The terms in (32), with (37), can be rearranged into the compact expression

$$\vec{E}^v(\vec{r}) \sim \frac{e^{-jkr}}{4\pi r} \bar{\bar{D}}^v \cdot \hat{u}, \tag{38}$$

where

$$\bar{\bar{D}}^v = j\bar{\bar{G}}^E(\vec{k}^v)B_1(\bar{k}_{z1s})B_2(\bar{k}_{z2s})$$
$$+ \bar{\bar{G}}^E(\vec{k}_q^{d,1})\frac{B_2(\bar{k}_{z2s})[F(a_q^2)-1]}{d_1 k(\cos\beta_{1,q}-\cos\beta_1)}$$
$$+ \bar{\bar{G}}^E(\vec{k}_p^{d,2})\frac{B_1(\bar{k}_{z1s})[F(b_p^2)-1]}{d_2 k(\cos\beta_{2,p}-\cos\beta_2)}$$
$$+ \frac{\bar{\bar{G}}^E(\vec{k}_{pq}^{FW})[T(a_q,b_p,w)-F(a_q^2)-F(b_p^2)+1]}{jd_1d_2k^2(\cos\beta_{1,q}-\cos\beta_1)(\cos\beta_{2,p}-\cos\beta_2)}. \quad (39)$$

This vertex-diffracted field incorporates the transition from a vertex-dominated spherical wave to an edge-dominated cylindrical wave, and it compensates for the discontinuities across the SBCs of edge-diffracted rays $\beta_{1,q} = \beta_1$ and $\beta_{2,p} = \beta_2$; the respective approximate parameters a_q and b_p vanish there (see equation (36)). The asymptotically dominant terms in the compensation mechanism at $\beta_{1,q} = \beta_1$ are those involving $F(a_q^2)$ and that reduced form of $T(a_q, b_p, w)$ which, for $\beta_2 \neq \beta_{2,p}$, behaves like $F(a_q^2)$. Analogous considerations apply to $\beta_{2,p} = \beta_2$. At the simultaneous intersection of the edge-diffracted conical $SBC_{1,2}$ and the truncated FW planar $SB_{1,2}$ (see Figure 3), both a_q and b_p vanish, and the corresponding $T(a_q, b_p, w)$ function transforms the vertex-induced field locally into a plane wave to match the Floquet wave. Finally, since the F and T functions tend to unity for large a_q and b_p, i.e., far from conical shadow boundaries, the quantities $[1 - F]$ and $[T(a_q, b_p, w) - F(a_q^2) - F(b_p^2) + 1]$ there are of asymptotic order $(kr)^{-1}$, whence the dominant asymptotic term is $j\bar{\bar{G}}^E(\vec{k}^v)B_1(\bar{k}_{z1s})B_2(\bar{k}_{z2s})$. Complete analytic tracking of this uniform asymptotic matching in overlapping shadow boundary transition regions is demonstrated by F. Capolino et al. (manuscript in preparation, 1999); also included by F. Capolino et al. is a generalized, and numerically more convenient, version of the Van der Waerden procedure which extracts a large enough number of poles to regularize the wavefield globally, thereby avoiding numerically inconvenient local patching. The extractions generate a corresponding number of additional terms in (39).

A more compact vertex diffraction coefficient $\bar{\bar{D}}^v$ can be obtained by a direct Pauli-Clemmow [*Kouyoumjian and Pathak*, 1974] asymptotic evaluation of the k_{z1}, k_{z2} integral (10), with deformation onto the local SDP (Figure 2). The asymptotics is performed uniformly with respect to the pole $k_{z1,q}$, $k_{z2,p}$ that is closest to the saddle point $(\bar{k}_{z1s}, \bar{k}_{z2s}) \equiv (k\cos\beta_1, k\cos\beta_2)$. This is done by multiplying and dividing the integrand in (10) by the product $W_{1,q}W_{2,p}$ of section 4.1. The slowly varying part $(8\pi^2 k_y)^{-1}B_1B_2\bar{\bar{G}}^E(\vec{k})/W_{1,q}W_{2,p}$ is removed from the integrand, thereby reducing the integral to the canonical form (35), which leads to (38) with the dyadic diffraction coefficient given instead of (39) by

$$\bar{\bar{D}}^v = j\bar{\bar{G}}^E(\vec{k}^v)B_1(\bar{k}_{z1s})B_2(\bar{k}_{z2s})T(a_q, b_p, w). \quad (40)$$

Depending on the position of the observer, measured in terms of the angular coordinates β_1, β_2, the indexes p, q always tag the two poles "closest" to the saddle point. Criteria for closeness will be given elsewhere (F. Capolino et al., manuscript in preparation, 1999). Results obtained from (40) are comparable to those obtained from (39) in a region "not too close" to the vertex of the array. Approaching the vertex, one sees that the diffraction coefficient (39) is superior; however, when augmented with the "slope" diffraction term, (40) and the globally regularized version of (39) perform comparably. Note that Van der Waerden accounts straightforwardly (by addition and subtraction) for any number of poles, whereas Pauli-Clemmow requires better tuning of the two nearest pole contributions.

5. Numerical Results

Numerical tests have been performed on a "large" square array of dipoles in order to validate the asymptotic solution in (31), using (38) with a (nine-term) globally regularized version of (39) (for details, see F. Capolino et al. (manuscript in preparation, 1999)). An element-by-element summation over the contribution from each dipole serves as a reference. From a variety of near-field scans carried out for different array parameters and dipole orientations, we have selected only one example because of space limitations. The quality of the analytic-numerical comparison in the example is typical of what we have found throughout. The 10×10 element test array of equiamplitude dipoles oriented along $\hat{u} = \hat{z}_1$ with interelement phasing $\gamma_1 = \gamma_2 = 0$ and period $d_1 = d_2 = 1.7\lambda$, $\lambda = 2\pi/k$, in both directions is shown in the inset of Figure 5. In a spherical coordinate system (r, θ, ϕ) with origin at the center of the array and polar axis perpendicular to the array plane, the array radiates a broadside ($\theta = 0°$) main beam, but owing to the large interelement distances d_1 and d_2, there are

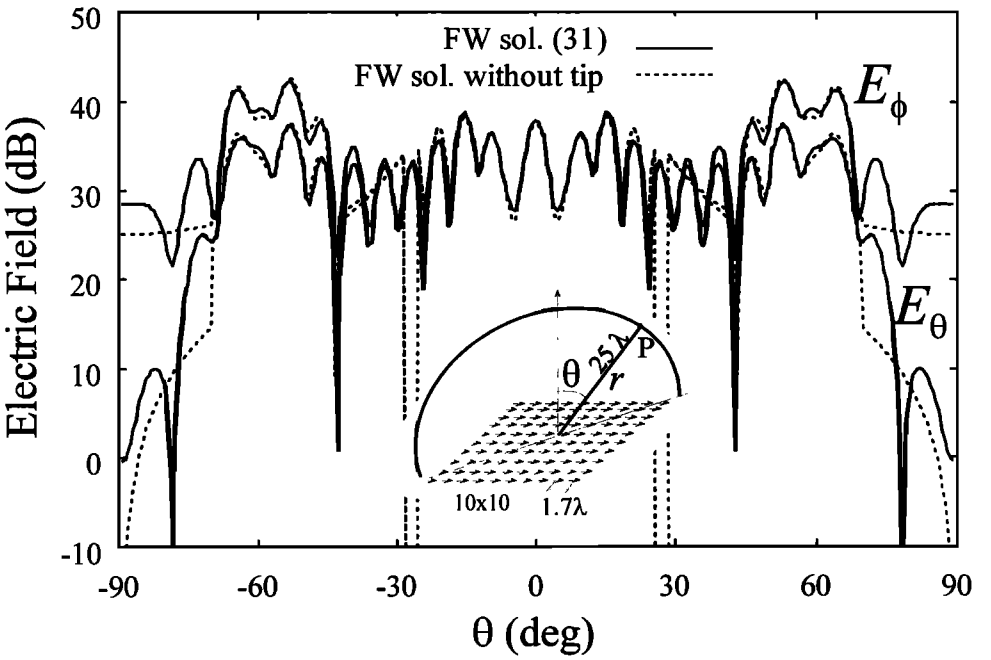

Figure 5. Electric field components E_θ and E_ϕ radiated by a 10 × 10 element array. On the scale of the plots the asymptotic FW solutions (31) with (38) (solid curves) are coincident with the element-by-element summation reference solution of dipole radiated fields. The solution (31) without vertex contribution (38) (dotted curves) is discontinuous when the observation scan crosses a SBC.

nine propagating FW_{pq}, with all combinations of $p = -1, 0, 1$ and $q = -1, 0, 1$. Also, there are three propagating diffracted waves $\tilde{E}_q^{d,1}$ with $q = -1, 0, 1$, arising from edge 1 since $|k_{z1,q}| < k$ for these q indexes; all other diffracted waves from edge 1 are radially evanescent and can be neglected. Thus, for edge 1, the p summation in (20) is over $p = -1, 0, 1$ (for every q considered) in order to compensate for propagating FWs with fixed q and $p = -1, 0, 1$; i.e., the three edge-1 diffracted waves can compensate for the disappearence of all nine propagating FWs at the shadow boundaries $\phi_{1,pq}^{SB}$ in (15) and (16). The same applies to the diffracted field from every other edge. Each of the three edge-1 diffracted fields has a SBC at $\beta_{1,q}^{SB}$, $q = -1, 0, 1$, given by (30) with (23). The vertex-1 diffracted field compensates for the disappearence of all these edge diffracted waves at their SBCs, thereby providing continuity of the total radiated field. All of these compensations are based on the Van der Waerden–globally regularized wave fields in section 4. The same mechanism applies to the diffracted field from each vertex of the square array. In Figure 5 the E_θ and E_ϕ total electric field components are plotted versus scan angle θ along a 45° arc at a distance $r = 25\lambda$ from the center of the array, thus passing close to two vertexes (see inset in Figure 5) so as to enphasize the vertex effect. The three maxima are related to the $FW_{-1,-1}$, FW_{00}, and FW_{11}. The dotted curves show the edge-truncated asymptotic FW and diffracted field solutions (31) without the vertex-diffracted field in (38). The solid curves show the complete asymptotic field in (31) with the globally regularized field in (38) as well as the reference solutions; both coincide on the scale of the drawing. The agreement between the complete asymptotic solution and the numerical reference solutions is quite satisfactory. The weaker radial electric component was also computed but has been omitted in order not to overtax the plots.

6. Concluding Remarks

In this paper we have presented a uniform asymptotic treatment of the canonical dyadic Green's function for a planar sectoral periodic array of parallel dipoles with linear interelement phasing and identical element amplitudes. This asymptotic construct not only speeds up the calculations when the array

Green's function (AGF) is used in a windowing approach [*Ishimaru et al.*, 1985; *Skrivervik and Mosig*, 1992], but also provides the basic guidelines for the formulation of a hybrid method where FW-modulated diffracted rays are used as basis functions in a method of moment scheme [*Neto et al.*, 1998]. We have synthesized the solution in terms of (1) the known phenomenologies of the two semi-infinite arrays corresponding to the nontruncated sector edges and (2) the new effects due to the vertex. Via the Van der Waerden–(steepest descent path) method, the formal sectoral array solution obtained in the two-dimensional spectral wavenumber domain has been reexpressed in an alternative rigorous form which is matched to subsequent asymptotic evaluation along the steepest descent paths in the complex wavenumber planes. The Van der Waerden architecture, which self-consistently combines these intertwined phenomenologies, has been presented, as has an approximate new canonical vertex diffraction function which achieves locally uniform patching from the vertex domain to the exterior edge-dominated regions; the patching can be avoided by a convenient globally regularized Van der Waerden form. The effectiveness of the globally regularized vertex diffraction function has been demonstrated by a numerical example which is typical of a large variety of other performed numerical tests. Details pertaining to the uniform local and global compensation mechanisms attributed to the vertex are to be presented separately (F. Capolino et al., manuscript in preparation, 1999). The results in this paper are relevant for the efficient calculation of the performance of rectangular phased arrays, as has been demonstrated previously for semi-infinite arrays [*Capolino et al.*, 2000a, b]. Moreover, the formulation has laid the foundation for an array-matched generalized geometrical theory of diffraction (GTD) which extends the concepts of conventional GTD for smooth configurations. On this basis the present high-frequency formulation can be extended to a nonuniformly excited array Green's function. When a smooth, slowly varying tapering function $f(z_1, z_2)$ of the excitation occurs over the entire domain of the array, the asymptotic AGF may be applied as well by invoking the local nature of high-frequency phenomena [*Felsen and Gago Ribas*, 1996]. A local infinite array can be defined for each array element as the periodic continuation of the investigated element with its local amplitude and phase excitation. This is equivalent to applying an adiabatic $f(z_1, z_2)$ modulation to each equivalent FW-matched continuous truncated aperture distribution. When the tapering function vanishes at the edge, significant slope diffraction contributions may arise, which are presently under investigation [see also *Nepa et al.*, 1999].

Acknowledgments. F. Capolino and S. Maci acknowledge partial support by the European Space Agency (ESA-ESTEC, Noordwijk, Netherlands) and by the Agenzia Spaziale Italiana (ASI). L. B. Felsen acknowledges partial support by the U.S. Naval Coastal Systems Center, Panama City, Florida, under ONR grant N61331-96-K-0028, and by the U.S.-Israel Binational Science Foundation, Jerusalem, Israel, under grant 95-00399. F. Capolino also acknowledges the Commission for Educational and Cultural Exchange between Italy and the United States for a Fulbright grant awarded in 1997 to conduct research at Boston University.

References

Albani, M., F. Capolino, S. Maci, and R. Tiberio, Diffraction at a thick screen including corrugations on the top face, *IEEE Trans. Antennas Propag.*, *45*(2), 277–283, 1997.

Capolino, F., and S. Maci, Simplified, closed-form expressions for computing the generalized Fresnel integral and their application to vertex diffraction, *Microwave Opt. Tech. Lett.*, *9*(1), 32–37, 1995.

Capolino, F., and S. Maci, Uniform high-frequency description of singly, doubly, and vertex diffracted rays for a plane angular sector, *J. Electromagn. Waves Appl.*, *10*, 1175–1197, 1996.

Capolino, F., M. Albani, S. Maci, and R. Tiberio, Diffraction from a couple of coplanar, skew wedges, *IEEE Trans. Antennas Propag.*, *45*(8), 1219–1226, 1997.

Capolino, F., M. Albani, S. Maci, and R. Tiberio, High-frequency analysis of an array of line sources on a truncated ground-plane, *IEEE Trans. Antennas Propag.*, *46*(4), 570–578, 1998.

Capolino, F., M. Albani, S. Maci, and L. B. Felsen, Frequency domain Green's function for a planar periodic semi-infinite phased array, part I, Truncated Floquet wave formulation, *IEEE Trans. Antennas Propag.*, in press, 2000a.

Capolino, F., M. Albani, S. Maci, and L. B. Felsen, Frequency domain Green's function for a planar periodic semi-infinite phased array, part II, Diffracted wave phenomenology, *IEEE Trans. Antennas Propag.*, in press, 2000b.

Carin, L., and L. B. Felsen, Time harmonic and transient scattering by finite periodic flat strip arrays: Hybrid Ray-Floquet mode-MoM algorithm, *IEEE Trans. Antennas Propag.*, *41*(4), 412–421, 1993.

Civi, O. A., P. H. Pathak, and H.-T. Chou, A hybrid UTD-MoM for efficient analysis from radiation/scattering from large finite planar arrays, in *Proceedings of the*

URSI International Symposium on Electromagnetic Theory, Thessaloniki, Greece, May 25–28, 1998, pp. 172–174, Int. Union of Radio Sci., Gent, Belgium, 1998.

Felsen, L. B., and L. Carin, Diffraction theory of frequency and time domain scattering by weakly aperiodic truncated thin wire gratings, *J. Opt. Soc. Am.*, *11*(4), 1291–1306, 1994.

Felsen, L. B., and E. Gago Ribas, Ray theory for scattering by two dimensional quasi-periodic plane finite arrays, *IEEE Trans. Antennas Propag.*, *44*(4), 375–382, 1996.

Felsen, L. B., and N. Marcuvitz, *Radiation and Scattering of Waves*, Prentice-Hall, Englewood Cliffs, N.J., 1973.

Hill, K. H., A UTD solution to the EM scattering by the vertex of a perfectly conducting plane angular sector, Ph.D. thesis, Dep. of Electr. Eng., Ohio State Univ., Columbus, 1990.

Ishimaru, A., R. J. Coe, G. E. Miller, and W. P. Geren, Finite periodic approach to large scanning array problems, *IEEE Trans. Antennas Propag.*, *33*(11), 1213–1220, 1985.

Jones, D. S., A uniform asymptotic expansion for a certain double integral, *Proc. R. Soc. Edinburgh, Sect. A*, *69*, 205–226, 1971.

Kouyoumjian, R. G., and P. H. Pathak, A uniform geometrical theory of diffraction for an edge in a perfectly conducting surface, *Proc. IEEE*, *62*(11), 1448–1461, 1974.

Maci, S., F. Capolino, and L. Felsen, Three-dimensional Green's function for planar rectangular phased dipole arrays, *Wave Motion*, in press, 1999.

Nepa, P., P. H. Pathak, O. A. Civi, and H.-T. Chou, A DFT based UTD ray analysis of the EM radiation from electrically large antenna arrays with tapered distribution, paper presented at the USNC/URSI National Radio Science Meeting, Orlando, Fla., July 11–16, 1999.

Neto, A., S. Maci, G. Vecchi, and M. Biagiotti, Full-wave analysis of a large rectangular array of slots, in *Proceedings of the IEEE-AP-S International Symposium*, pp. 21–26, IEEE Press, Piscataway, N.J., 1998.

Skrivervik, A., and J. Mosig, Finite planed array of microstrip patch antennas: The infinite array approach, *IEEE Trans. Antennas Propag.*, *40*(5), 579–582, 1992.

Van der Waerden, B. L., On the method of saddle points, *Appl. Sci. Res., Ser. B*, *2*, 33–45, 1951.

F. Capolino and S. Maci, Department of Information Engineering, University of Siena, Via Roma 56, 53100 Siena, Italy. (capolino@ing.unisi.it)

L. B. Felsen, Department of Aerospace and Mechanical Engineering, Boston University, 110 Cummington Street, Boston, MA 02215.

(Received January 26, 1999; revised September 10, 1999; accepted September 30, 1999.)